Visualizing depth and thickness of a local blood region in skin tissue using diffuse reflectance images

Izumi Nishidate
Yamagata University
Department of Bio-system Engineering
4-3-16, Jonan, Yonezawa
Yamagata 992-8510, Japan

Takaaki Maeda
Yoshihisa Aizu
Muroran Institute of Technology
Department of Mechanical System Engineering
27-1, Mizumoto, Muroran
Hokkaido 050-8585, Japan

Kyuichi Niizeki
Yamagata University
Department of Bio-system Engineering
4-3-16, Jonan, Yonezawa
Yamagata 992-8510, Japan

Abstract. A method is proposed for visualizing the depth and thickness distribution of a local blood region in skin tissue using diffuse reflectance images at three isosbestic wavelengths of hemoglobin: 420, 585, and 800 nm. Monte Carlo simulation of light transport specifies a relation among optical densities, depth, and thickness of the region under given concentrations of melanin in epidermis and blood in dermis. Experiments with tissue-like agar gel phantoms indicate that a simple circular blood region embedded in scattering media can be visualized with errors of 6% for the depth and 22% for the thickness to the given values. *In-vivo* measurements on human veins demonstrate that results from the proposed method agree within errors of 30 and 19% for the depth and thickness, respectively, with values obtained from the same veins by the conventional ultrasound technique. Numerical investigation with the Monte Carlo simulation of light transport in the skin tissue is also performed to discuss effects of deviation in scattering coefficients of skin tissue and absorption coefficients of the local blood region from the typical values of the results. The depth of the local blood region is over- or underestimated as the scattering coefficients of epidermis and dermis decrease or increase, respectively, while the thickness of the region agrees well with the given values below 1.2 mm. Decreases or increases of hematocrit value give over- or underestimation of the thickness, but they have almost no influence on the depth. [DOI: 10.1117/1.2798703]

Keywords: skin tissue; hemoglobin; melanin; isosbestic wavelength; diffuse reflectance; Monte Carlo simulation; absorbance.

Paper 06283RR received Oct. 11, 2006; revised manuscript received Apr. 27, 2007; accepted for publication May 29, 2007; published online Oct. 19, 2007.

1 Introduction

The depth profile of a local blood region in skin tissue is an important parameter in clinical diagnosis and treatments in dermatology. Various vascular malformations have their own histopathological pattern throughout the depths of lesions and are classified by the depth profile of lesions.[1] In laser treatment of port wine stains, the depth profile of a lesion may be used to optimize the pulse duration and radiant exposure of light.[1–7] Conventional methods such as magnetic resonance imaging and ultrasound imaging have been utilized for differential diagnoses of such diseases,[1] but they often provide insufficient contrast between different types of soft tissue.

Several techniques based on light-tissue interactions have been reported for profiling the depth of local blood region in skin tissue. Nelson et al.[8] reported a technique for imaging the depth distribution of port wine stains using a fast infrared focal plane array camera that acquires the infrared emission due to temperature rise created by the absorption of pulsed laser radiation in blood vessels. An optoacoustic technique has also been studied for imaging a strongly absorbing region such as localized blood or bloody tissue. This technique detects a pressure wave generated by thermoerastic expansion of an absorbing object within tissue, due to a temperature rise that is induced by pulsed laser radiation. Time-resolved pressure wave signals are used to reconstruct depth profiles of the object. Various methods using the optoacoustic technique have been studied to probe depth profiles of port wine stain lesions,[7] forearm veins,[9] breast tumors,[10] and mouse brain.[11] Although those techniques are promising for *in-vivo* imaging of subsurface absorbing regions, all of them require a pulsed laser source, and thus, can be costly for practical uses at present.

Diffuse reflectance measurements for skin tissue can be achieved with a simple apparatus, and thus have been used to evaluate physiological information of tissue, such as melanin and hemoglobin in skin tissue.[12–20] To deduce structural information such as the depth of a blood region, a few methods[21–23] using diffusely backscattered light were also reported. Iwai and Kimura[21] introduced the maximum path length for the path-length probability distribution of light backscattered from an optically turbid medium. They deduced

Address all correspondence to Yoshihisa Aizu, Mechanical Systems Engineering, Muroran Institute of Technology, 27-1, Mizumoto - Muroran, Hokkaido 050-8585 Japan; Tel: 81 143 46 5348; Fax: 81 143 46 5360; E-mail: aizu@mmm.muroran-it.ac.jp

1083-3668/2007/12(5)/054006/12/$25.00 © 2007 SPIE

the depth, via a numerical model of light propagation, by assuming that the maximum path length was proportional to the depth and related to measured integrated backscattered intensity. This approach, however, suffers from misestimation of the depth due to variation in the maximum path length, which is due to the oxygenation of hemoglobin. Furthermore, scanning of a source and detector set or sample is required for imaging. Jacques, Saidi, and Tittel[22] reported an approach utilizing a ratio of optical densities at two isosbestic wavelengths of hemoglobin (420 and 585 nm), which make it possible to estimate the average depth of capillary network regions in dermis, independently of the oxygenation. However, it may be affected by the variation of melanin content among individuals, and has not been implemented yet for imaging modality.

We have previously proposed a method,[23] based on the approach by Jacques, Saidi, and Tittel, for imaging the depth of a local blood region such as veins under skin tissue. Diffuse reflectance images of skin surfaces covering a local blood region, together with the surrounding skin site at the two isosbestic wavelengths, were acquired by a charge-coupled device (CCD) camera. The concentration of melanosomes in epidermis and hemoglobin in dermis estimated from the reflectances on the surrounding skin site was used to compensate variation in the ratio of optical densities among individuals. In the present study, we expand the method for visualization of both depth and thickness of a local blood region using reflectance images acquired at three isosbestic wavelengths of 420, 585, and 800 nm. A ratio of optical densities at 420- and 800-nm wavelengths is newly introduced to obtain the thickness of a blood region. Monte Carlo simulation of light transport for layered skin tissue structure specifies a relation among optical densities, depth, and thickness of the region under given concentrations of melanin in epidermis and blood in dermis. Experiments with tissue-like agar gel phantoms having a circular blood inclusion and *in-vivo* imaging for human veins under skin tissue are performed to confirm the ability of the method. Errors expected in the estimated depth and thickness of the blood region due to variations in scattering coefficients of skin tissue and hematocrit of blood are numerically investigated for diffuse reflectance samples generated by Monte Carlo simulation.

2 Principle

2.1 *Layered Skin Tissue Model for Light Transport*

In this study, we treat a simple layered skin tissue model shown in Fig. 1, where site A consists of planar epidermis and dermis, representing the common skin tissue site. Usually, the main chromophores in this site are melanosomes containing melanin at the basal layer of epidermis and hemoglobin in blood within the superficial plexus in dermis. For convenience, it is assumed that melanosomes and hemoglobin are distributed homogeneously over the epidermis and dermis, respectively. Site B, contiguous to site A, is assumed to have a local blood region within the dermis. This blood region is a target of estimation in this study.

To simulate diffuse reflectance from the skin tissue, we use the Monte Carlo code developed by Wang, Jacques, and Zheng,[24] in which the diffuse reflectance from multilayered tissue can be calculated. This code utilizes the Heney-Greenstein phase function. Each epidermis, dermis, and local

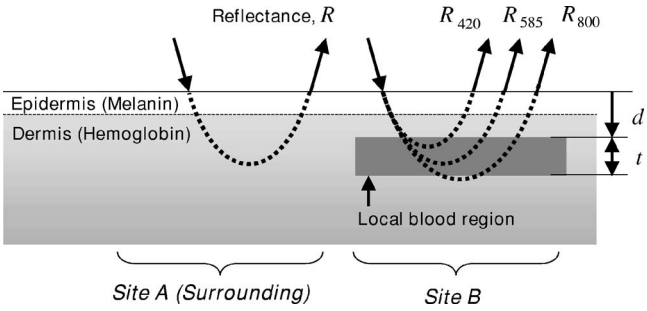

Fig. 1 Multilayered skin tissue model. Site A represents the common skin region and site B has a local blood region within dermis.

blood region can be characterized by the scattering coefficient $\mu_s(\lambda)$ mm^{-1}, absorption coefficient $\mu_a(\lambda)$ mm^{-1}, anisotropy factor $g(\lambda)$, and refractive index $n(\lambda)$ as a function of wavelength λ nm and thickness t mm. Table 1 shows the optical parameters used for the Monte Carlo simulation in this study. The absorption coefficient of epidermis $\mu_{a,\mathrm{epi}}(\lambda)$ depends on the volume concentration of melanosomes in epidermis C_m. We assumed that the absorption coefficient $\mu_{a,m}(\lambda)$ of a standard amount of melanosomes given in the literature[25] corresponds to that of the epidermis in the case of C_m=100%. Then we derived the corresponding absorption coefficients of epidermis $\mu_{a,\mathrm{epi}}(\lambda)$ for ten different cases of C_m=1 to 10% at intervals of 1%, by simply proportioning it to $\mu_{a,m}(\lambda)$ as

$$\mu_{a,\mathrm{epi}}(\lambda) = C_m \times \mu_{a,m}(\lambda). \quad (1)$$

Since the proposed method relies on the reflectance at isosbestic wavelengths, the absorption coefficient of dermis is independent of the oxygenation of blood. The absorption and

Table 1 Optical parameters used in the Monte Carlo simulation for the skin tissue model.

Optical parameter	Wavelength (nm)		
	420	585	800
Absorption coefficient of melanosomes $\mu_{a,m}$(mm^{-1})	121.3	40.5	14.4
Absorption coefficient of blood $\mu_{a,b}$(mm^{-1})	230.6	18.4	0.42
Scattering coefficient of blood $\mu_{s,b}$(mm^{-1})	57.9	83.6	75.2
Scattering coefficient of epidermis and dermis $\mu_{s,\mathrm{epi}}$, $\mu_{s,\mathrm{der}}$(mm^{-1})	33.4	14.9	9.3
Anisotropy factor of blood g_b	0.98	0.98	0.98
Anisotropy factor of epidermis and dermis g_{epi}, g_{der}	0.74	0.79	0.85

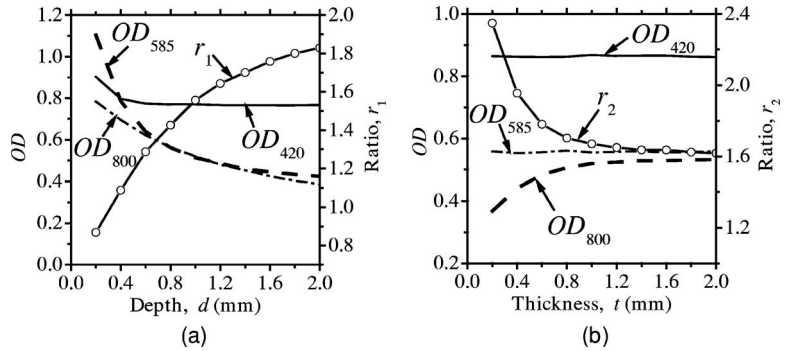

Fig. 2 (a) Dependence of OD_{420}, OD_{585}, and their ratio r_1, and OD_{800} on the depth d. (b) Dependence of OD_{420}, OD_{800}, and their ratio r_2, and OD_{585} on the thickness t, derived by Monte Carlo simulations.

scattering of a local blood region were set to be those of blood with 44% hematocrit (Hct). The absorption coefficient $\mu_{a,b}(\lambda)$ of blood was derived as

$$\mu_{a,b}(\lambda) = 2.303 \times e_{\mathrm{hb}}(\lambda) \times G/W, \tag{2}$$

where $e_{hb}(\lambda)$ liter/(mol·cm) is the molar extinction coefficient of hemoglobin reported by Prahl.[26] The hemoglobin concentration in blood with 44% hematocrit G g/liter and the gram molecular weight of hemoglobin W g/mol were set to be 150 and 65,500, respectively. In a previous study, Roggan et al.[27] indicated that the scattering coefficients of blood increase linearly with hematocrit if Hct$<$50%. Therefore, the scattering coefficient of blood with 44%-Hct, $\mu_{s,b}(\lambda, \mathrm{Hct}=44\%)$ was scaled based on the data reported for Hct=5% originally by Roggan et al.,[27]

$$\mu_{s,b}(\lambda, \mathrm{Hct}=44\,\%) = \mu_{s,b}(\lambda, \mathrm{Hct}=5\,\%) \times (44/5). \tag{3}$$

We regarded that the anisotropy factor of blood at 633 nm was 0.98 for Hct=44% in the results by Roggan et al.[27] Furthermore, the anisotropy factors of blood at 420, 585, and 800 nm are almost equal to that at 633 nm in their results. Therefore, the anisotropy factor g_b of blood was set to be 0.98 for 420, 585, and 800 nm in this study.

The scattering coefficients $\mu_{s,\mathrm{epi}}(\lambda)$ and $\mu_{s,\mathrm{der}}(\lambda)$ of epidermis and dermis, respectively, were approximated by using the same relation given by Jacques,[28]

$$\mu_{s,\mathrm{epi}}(\lambda) = \mu_{s,\mathrm{der}}(\lambda) = (2 \times 10^5 \times \lambda^{-1.5} + 2 \times 10^{12} \times \lambda^{-4})/(1-g), \tag{4}$$

The anisotropy factors of $g_{\mathrm{epi}}(\lambda)$ and $g_{\mathrm{der}}(\lambda)$ epidermis and dermis, respectively, were calculated as

$$g_{\mathrm{epi}}(\lambda) = g_{\mathrm{der}}(\lambda) = 0.62 + \lambda \times 0.29, \tag{5}$$

which has been reported by Gemert et al.[29] The absorption coefficient of dermis $\mu_{a,\mathrm{der}}(\lambda)$ was obtained by averaging the absorption coefficient of blood proportionally according to their volume concentration or percentage C_b as,

$$\mu_{a,\mathrm{der}}(\lambda) = C_{\mathrm{b}} \times \mu_{a,b}(\lambda). \tag{6}$$

Therefore, the absorption coefficient of blood is assumed to be that of blood in the case of C_b=100%. The volume concentration of blood is usually different among individuals and may change due to the physiological condition of tissue. Jacques[28] has introduced that the typical volume concentration of blood in dermis is 0.2% in the skin model where the blood distributed homogeneously over the dermis. This value of 0.2% has been referred in the Monte Carlo calculation model of skin tissue reported by Dai et al.[30] Taking the variability of the blood concentration in dermis into account, the absorption coefficients of dermis were derived for three different concentrations of C_b=0.2, 0.4, and 0.6%, at 420-, 585-, and 800-nm wavelengths. We define the depth d as a distance from the skin surface to the upper surface of the local blood region. Both the depth d and thickness t of the blood region were set to be from 0.2 to 2 mm at intervals of 0.2 mm. The thicknesses t_e and t_d of epidermis and dermis were assumed to be 0.06 and 4.94 mm, respectively. The refractive index n for each layer is assumed to be 1.4 at the three wavelengths.[18,19] For each wavelength, therefore, the combination of C_m and $C_b$values gave 30 diffuse reflectance data for site A, whereas that of C_m, C_b, d, and t took 3000 data for site B. The total calculation time for reflectance samples was roughly 1.5 h for site A, whereas it was 230 h for site B, using Athlon CPU, 2.0 GHz.

2.2 *Empirical Formulas for the Depth and Thickness*

Figure 1 also illustrates the concept of the method. An optical density OD at wavelength λ nm can be expressed with a diffuse reflectance of skin tissue R as,

$$OD(\lambda) = -\log_{10} R(\lambda). \tag{7}$$

In Fig. 1, $OD(\lambda)$ for site A represents the absorption of light due to melanosomes in epidermis and hemoglobin in dermis. When a local blood region exists in skin tissue as site B, light propagated in the tissue is absorbed by hemoglobin in the region as well. Then $OD(\lambda)$ for site B may depend on the depth d and thickness t of the region. For a visible to near-infrared wavelength range, both the scattering and absorption of light in skin tissue is stronger at the shorter wavelength than at the longer wavelength. Therefore, the shorter wave-

length light is backscattered mainly from the superficial layer such as epidermis and reticular dermis, whereas the longer wavelength light penetrates into the deeper region of dermis.

Figures 2(a) and 2(b) show the dependence of $OD(\lambda)$ on the depth d and thickness t, respectively, derived from the Monte Carlo simulations at site B in Fig. 1. In this case, the volume concentrations of melanosomes in epidermis and blood in dermis were C_m=4.0% and C_b=0.2%, respectively. In Fig. 2(a), OD_{585} and OD_{800} are decreased as the blood region becomes deep, whereas OD_{420} shows decrease only when the blood region with t=1.0 mm is shallow. In Fig. 2(b), OD_{800} is first increased and then becomes constant as the blood region at d=1.0 mm becomes thick, whereas OD_{420} and OD_{585} are almost constant with respect to the thickness. Thus, OD_{800} depends on both the depth d and thickness t. Therefore, we can estimate the depth d in the range of 0.2 to 2 mm from OD_{420} and OD_{585} with no influence of thickness t. In this case, the ratio $r_1=OD_{420}/OD_{585}$, which is increased as the depth d becomes large,[22,23] can be used to determine the depth d. Once the depth of the local blood region is specified, OD_{800} is used to estimate the thickness t without the influence of depth d. In this case, a ratio $r_2=OD_{420}/OD_{800}$, which is decreased as the thickness t becomes large, is available for determination of the thickness t. It should be noted that the curve $r_1(d)$ varies according to values of C_m and C_b, but it is not significantly affected by thickness t in a range of 0.2 to 2 mm. On the other hand, the curve $r_2(t)$ depends on values of C_m, C_b, and also d.[31] These parameters C_m, C_b, and d are usually different among individuals, and also change due to physiological or structural conditions of tissue. In this method, we first estimate C_m and C_b from measured OD values, and then specify the ratio $r_1(d)$ as a function of d to determine the depth d. The estimated values of C_m, C_b, and d are used to specify the ratio $r_2(t)$ as a function of t, and finally, we obtain the thickness t. The other parameters μ_s, g, and n, which may also affect the diffuse reflectance, are assumed to be known and constant, since their determination is currently unavailable by the proposed method. Some discussions are made in Sec. 4.3 on the effects of the scattering coefficient of skin tissue and the hematocrit of a blood region on the results of depth and thickness.

Figure 3 describes an estimation process for imaging the depth and thickness of a local blood region. First of all, we take reflectance images of skin surface, covering a local blood region (site A), together with the surrounding skin site (site B) at the three isosbestic wavelengths, 420, 585, and 800 nm. These three reflectance images, R_{420}, R_{585}, and R_{800}, are converted into the optical density images OD_{420}, OD_{585}, and OD_{800}, respectively. The concentration images of C_m and C_b are then derived from OD values according to the modified Beer-Lambert law. In this case, OD at wavelength λ is expressed as

$$OD(\lambda) = C_{\mathrm{m}} e_{\mathrm{m}}(\lambda) l_{\mathrm{e}}(\lambda) + C_{\mathrm{b}} e_{\mathrm{b}}(\lambda) l_{\mathrm{d}}(\lambda) + OD_0(\lambda), \quad (8)$$

where e, l, and OD_0 are the extinction coefficient, mean path length, and attenuation due to scattering, respectively. Subscripts m, b, e, and d indicate melanosomes, blood, epidermis, and dermis, respectively. A linear conversion of Eq. (8) for λ=420 and 585 nm yields

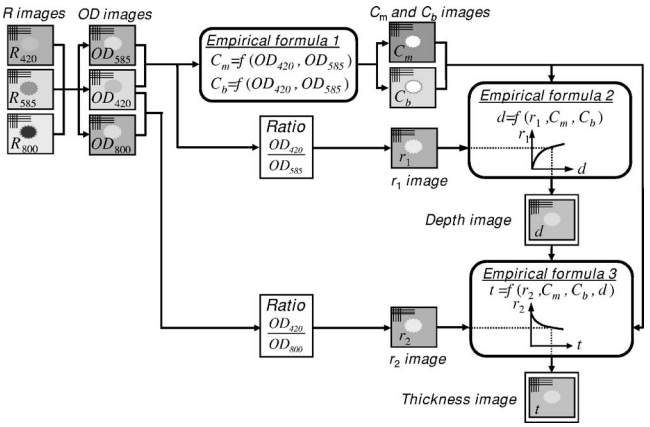

Fig. 3 Estimation process for the depth and thickness of a local blood region.

$$C_{\mathrm{m}} = a_{\mathrm{m}1} OD_{420} + a_{\mathrm{m}2} OD_{585} + a_{\mathrm{m}0}, \quad (9)$$

$$C_{\mathrm{b}} = a_{\mathrm{b}1} OD_{420} + a_{\mathrm{b}2} OD_{585} + a_{\mathrm{b}0}, \quad (10)$$

where a_{mi} and $a_{bi}(i=0,1,2)$ are derived in advance by the multiple regression analysis (MRA) of given values of C_m and C_b, and the corresponding Monte-Carlo results of OD_{420} and OD_{585} at site A.

Next, the function $r_1(d)$ is approximated by an exponential function as $r_1(d)=r_{1,0}+A_1\exp(-d/u_1)$, and thus,

$$d(r_1) = -u_1 \ln[(r_1 - r_{1,0})/A_1], \quad (11)$$

$$r_{1,0} = \alpha_1 \cdot C_m + \alpha_2 \cdot C_b + \alpha_0, \quad (12)$$

$$A_1 = \beta_1 \cdot C_m + \beta_2 \cdot C_b + \beta_0, \quad (13)$$

$$u_1 = \gamma_1 \cdot C_m + \gamma_2 \cdot C_b + \gamma_0, \quad (14)$$

where $r_{1,0}$, A_1, and u_1 are approximated as simple linear functions of C_m and C_b, and coefficients of α_i, β_i, and $\gamma_i(i=0,1,2)$ were optimized by MRA for the Monte-Carlo results of the $r_1(d)$ at site B. By applying Eq. (11) to each pixel of the r_1 image, a depth image is reconstructed. Then, the function $r_2(t)$ is also approximated by another exponential function $r_2(t)=r_{2,0}+A_2\exp(-d/u_2)$, and thus,

$$t(r_2) = -u_2 \ln[(r_2 - r_{2,0})/A_2], \quad (15)$$

$$r_{2,0} = \delta_1 \cdot C_m + \delta_2 \cdot C_b + \delta_3 \cdot d + \delta_0, \quad (16)$$

$$A_2 = \phi_1 \cdot C_m + \phi_2 \cdot C_b + \phi_3 \cdot d + \phi_0, \quad (17)$$

$$u_2 = \sigma_1 \cdot C_m + \sigma_2 \cdot C_b + \sigma_3 \cdot d + \sigma_0, \quad (18)$$

where $r_{2,0}$, A_2, and u_2 are approximated as functions of C_m, C_b, and d, and coefficients of δ_j, ϕ_j, and σ_j $(j=0,1,2,3)$ were determined by MRA for the Monte-Carlo results of $r_2(t)$ at site B. By applying Eq. (15) to each pixel of the r_2 image, a thickness image is finally reconstructed. Equations

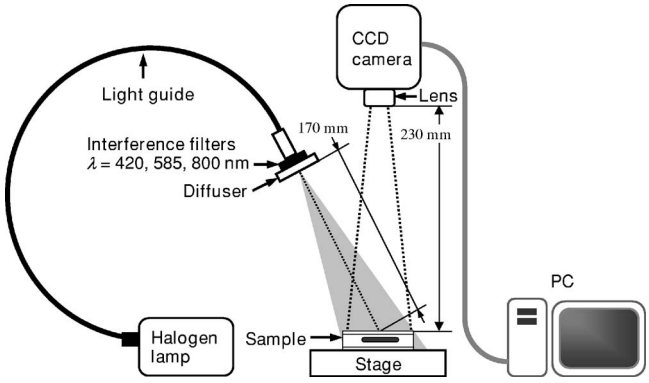

Fig. 4 Measuring apparatus for the method.

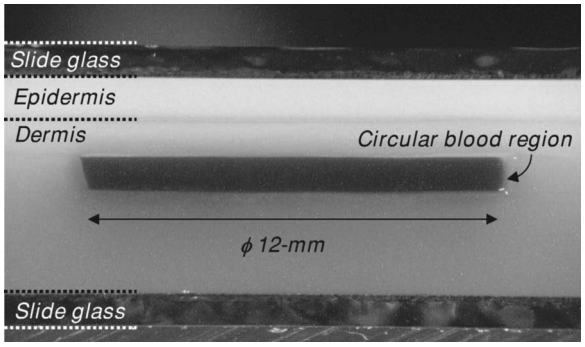

Fig. 5 Cross sectional photograph of a tissue-like agar gel phantom.

(8) through (18) are our empirical formulas and are established before measurements.

3 Materials and Method

3.1 *Measuring Apparatus*

Figure 4 simply shows a measuring apparatus. A 150-W halogen-lamp light source (LA-150SAE, Hayashi, Japan) illuminates the surface of a sample via a light guide, interference filter, and diffuser. The light source covers a range from visible to near-infrared wavelength. The angle of illumination is approximately 45 deg with respect to the sample surface. The diffuser is used to reduce irregular intensity distribution of the exiting light. By using three interference filters of 420-, 585-, and 800-nm wavelengths with 10-nm spectral full-width at half-maximum (CVI Laser LLC, Albuquerque, NM, USA) alternately, diffuse reflectance images at the three isosbestic wavelengths are acquired by a 16-bit cooled CCD camera (BS-40, Bitran, Japan) with a camera lens (Pentax/Cosmicar, Japan; f 16 mm, 1:1.4), on the basis of reflected intensities from a spectralon white standard with 99% reflectance (SRS-99-020, Labsphere Incorporated, North Sutton, NH, USA) and six self-made grayscale phantoms ranging from 1 to 55% reflectance. The grayscale phantoms were prepared using agar gels with Intralipid 10% solution (Fresenius Kabi AB, Uppsala, Sweden) and India ink (Kaimei Incorporated, Saitama, Japan), and used to compensate the nonlinear sensitivity of the camera with respect to the input light intensity. The integration time of the CCD camera for each reflectance image was <1.3 s, although it is expected to reduce the time by optimizing the arrangement of the optical system. Field of view of the system was 92×69 mm^2 with 386×290 pixels. The reflectance images are stored in a personal computer and analyzed according to the estimation process described in Fig. 3. In this study, human skin tissue on the inner forearm of a Japanese adult male and tissue-like agar gel phantoms were employed as subjects for experiments.

3.2 *Tissue-Like Agar Gel Phantoms*

Figure 5 shows a cross sectional photograph of the phantom. The phantom with an area of 45×26 mm^2 consists of epidermis and dermis layers containing a 12-mm-diam circular region with oxygenated blood. The agar solution was prepared by diluting agar powder (Ina Food Industrial Incorporated, Ina, Japan) with saline at a weight ratio of 0.8%. To set the scattering condition, Intralipid 10% solution (Fresenius Kabi AB, Sweden) was added to the agar solution. The resultant solution was used as a base material for epidermis and dermis layers. Coffee solution was introduced as melanosome substitute into the base material, and this mixture was used to make an epidermis layer. In the phantom experiments, therefore, a notation C_c is used instead of C_m. An oxygenated dermis layer was made by adding a small amount of fully oxygenated horse blood with Hct=44% to the base material. The volume concentration of coffee solution was set to be $C_c=1$ to 10% at an interval of 1%, while that of blood was to be $C_b=0.2$, 0.4, and 0.6%. For the local blood region, an oxygenated blood material was prepared by mixing the agar solution with fully oxygenated red blood cells of horse blood in Hct=20%. In this study, it was difficult to make the local blood region with 44% hematocrit by agar. A phantom with a more dense blood region is under development, and experiments using such a phantom will be reported in the near future. The volume concentrations C_c and C_b of coffee solution in the epidermis layer and blood in the dermis layer were set to be 5.0 and 0.4%, respectively. All these layers were hardened in various molds having the required thickness, size, and shape by being cooled at about 5.5 °C for 30 min. The epidermis layer, dermis layer, and blood region were 1.0, 5.0, and 1.0 mm in thickness, respectively. The depth of a local blood region were set to be $d=1.5$, 2.0, and 3.0 mm, whereas its thickness was to be $t=0.5$, 1.0, 1.5, and 2.0 mm. These layers were then piled to be a multilayered phantom, which was put between two slide glasses, as shown in Fig. 5. The slide glass on the epidermis layer was naturally coupled to the phantom by a drop of water.

The empirical formulas should be prepared for phantom experiments, separately from *in-vivo* experiments. Diffuse reflectance samples at wavelengths of 420, 585, and 800 nm were generated by using the Monte Carlo simulations for the phantom conditions. Optical parameters of $\mu_s(\lambda)$ mm^{-1} and $\mu_a(\lambda)$ mm^{-1} for the phantom were determined by the inverse Monte Carlo method for measured diffuse reflectance and total transmittance.[18,19,27] The refractive index n for each layer was assumed to be 1.33 at the three wavelengths. The anisotropy factor g of Intralipid 10%[32] was used for the epidermis and dermis layers, while that of whole blood[27] was introduced for the blood layer. To compensate difference in the thickness of epidermis between the phantom and human skin, μ_s and μ_a

Table 2 Optical parameters used in the Monte Carlo simulation for phantoms with C_c=5.0%, C_b=0.4%, and Hct=20% of a local blood region.

Wavelength λ	Layer	μ_s (mm^{-1})	μ_a (mm^{-1})	g (-)
420 nm	Epidermis	8.1	0.11	0.86
	Dermis	3.7	0.5	0.86
	Blood	9.04	13.1	0.98
585 nm	Epidermis	3.5	0.01	0.76
	Dermis	3.2	0.07	0.76
	Blood	7.1	9.9	0.98
800 nm	Epidermis	1.62	0.007	0.64
	Dermis	1.43	0.005	0.64
	Blood	152.4	0.299	0.99

were controlled so that *OD* of the phantom came close to that of human skin by regulating the concentration of Intralipid and coffee solution. Table 2 shows typical optical parameters for the phantom with C_c=5%, C_b=0.4%, and Hct=20% of the local blood region. Details of preparation for the phantom and its optical properties have been publishedpreviously.[18,19] Both the depth d and thickness t of the blood region were set to be from 0.2 to 2 mm at intervals of 0.2 mm. For each wavelength, therefore, the combination of C_c and C_b gave 30 diffuse reflectance data for site A, whereas that of C_c, C_b, d, and t took 3000 data for site B. According to the derivation process described in Secs. 2.1 and 2.2, the empirical formulas for the phantom were obtained.

3.3 *Method for Numerical Investigation*

As we mentioned before, the proposed method assumes that the scattering coefficients $\mu_s(\lambda)$ mm^{-1} of epidermis and dermis and the hematocrit Hct% or absorption coefficient $\mu_a(\lambda)$ mm^{-1} of blood are known, and typical values published in literatures are used to derive the empirical formulas. However, these values have subject-to-subject variability and may change due to the physiological or structural condition of tissue. To investigate the effect of variation in scattering coefficients of the tissue and in hematocrit of the blood on the results, we performed numerical estimation for diffuse reflectance samples generated by the Monte Carlo simulation when each value of $\mu_s(\lambda)$ mm^{-1} and Hct% had some variations. For test samples, values of $\mu_s(\lambda)$ mm^{-1} were set with −20, −10, 10, and 20% decrement or increment of the value listed in Table 1, whereas those of Hct% in both dermis and a local blood region were with −10, −20, 14, and 25% of them.

4 Results and Discussion

4.1 *Experiments for Phantoms*

To investigate the feasibility of the method, we carried out experiments using tissue-like agar gel phantoms. Figure 6

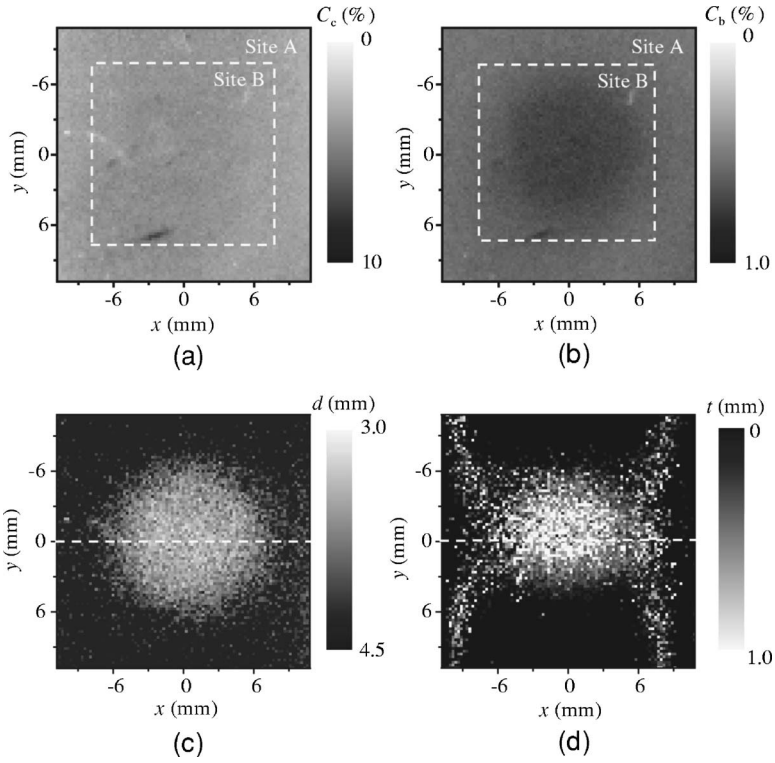

Fig. 6 Concentration images of (a) coffee in epidermis and (b) blood in dermis, obtained from the phantom. Each image was divided into site A (without a blood region) and site B (with a blood region). Images of (c) depth and (d) thickness of a circular blood region were obtained from the phantom.

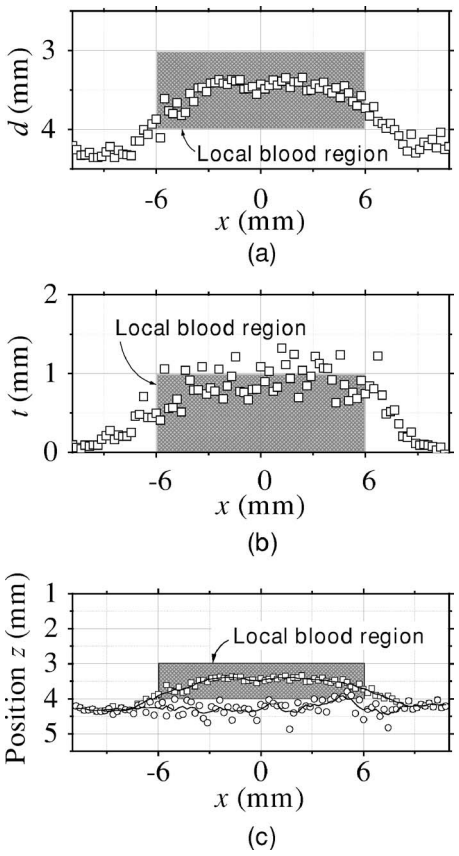

Fig. 7 Profiles of (a) depth and (b) thickness corresponding to the dashed line in Figs. 6(c) and 6(d), respectively. (c) Outline profile of the blood region reconstructed from (a) and (b). Squares and circles in (c) denote the upper surface (depth profile) and the lower surface (sum of depth and thickness profiles), respectively.

shows typical results of images obtained from the phantom having a local blood region for [Fig. 6(a)] volume concentration of coffee in the epidermis layer C_c and [Fig. 6(b)] that of blood in the dermis layer C_b, [Fig. 6(c)] depth d, and [Fig. 6(d)] thickness t. We divided the image into sites A and B by a dashed line in Figs. 6(a) and 6(b). For site A, the average values of C_c and C_b were estimated by Eqs. (9) and (10) to be 3.17 and 0.45%, respectively, whereas the original values of C_c and C_b were 5.0 and 0.4% when the phantom was made. These average values of C_c and C_b were used to obtain images of Figs. 6(c) and 6(d), which demonstrate depth and thickness distributions of the circular blood region. The original values of depth and thickness of the blood region set in the phantom were $d=3.0$ mm and $t=1.0$ mm, respectively. It should be noted that the border of blood region is blurred in the results of both depth and thickness. This is mainly due to diffusion of light from the surrounding dermis to the blood region. The bright areas spreading to the four corners in the thickness image of Fig. 6(d) seem to be artifacts. Similar artifacts were also observed in the original reflectance image at 800 nm, whereas the reflectance images at 420 and 585 nm did not have them (not shown here). Therefore, the artifacts were observed in the thickness image but not in the depth image. The source of these artifacts has not been clearly identified yet. We consider that it is probably due to unexpected light reflected from the slide glass under the phantom or light penetrated from both side faces of the phantom, because the penetration of light at 800 nm could be larger than that at 420 or 585 nm for the phantom. This needs further investigation in future work.

Figures 7(a) and 7(b) demonstrate profiles of d and t along with dashed lines in Figs. 6(c) and 6(d), respectively. The estimated depth has error of about 0.3 mm corresponding to 10% of the given value, which is still large for future clinical use and should be improved mainly by more accurate estimation of C_c and C_b. The estimated thickness is close to the original value on average, but it has fluctuation. These profiles are then combined together and reconstructed as shown in Fig. 7(c). Squares and circles in Fig. 7(c) denote estimated plots of the upper surface (depth profile) and the lower surface (sum of depth and thickness profiles), respectively. The estimated outline of the blood region roughly corresponds to the original, but blurring effect occurs in the border again. Figure 8 shows comparison between the estimated and original values of Fig. 8(a) depth d and Fig. 8(b) thickness t. The estimated values are proportional to the original values, but some errors are shown when the blood region is deep and thick. The errors of depth and thickness correspond to 6.1 ± 2.6 and $22.0\pm14.4\%$ of the given values, respectively. These errors can be caused by properties of the functions $r_1(d)$ and $r_2(t)$ becoming gradually insensitive to d and t with increasing depth and thickness, respectively, as shown in Figs. 2(a) and 2(b). Therefore, measurable ranges of the depth and thickness

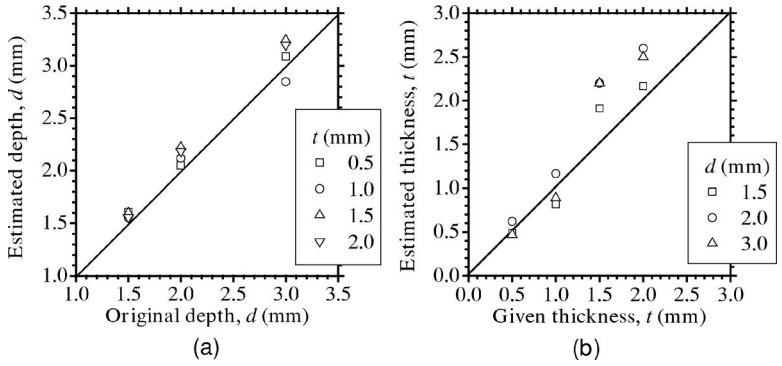

Fig. 8 Comparison of the estimated and original values for (a) depth and (b) thickness of a circular blood region in the phantom experiments.

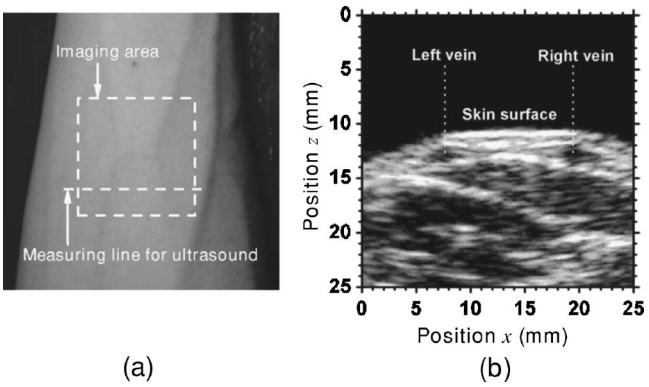

Fig. 9 (a) Photograph of a measured skin region including veins and (b) example of a classical ultrasound image (B-mode) along with the dashed line in (a).

are essentially limited by the characteristics of $r_1(d)$ and $r_2(t)$.

4.2 *Experiments for Human Veins*

To investigate the applicability of the method to *in-vivo* measurements, we next conducted experiments for human skin tissue, including veins. To compare results of the proposed method with the conventional technique, ultrasound imaging of the same veins was also conducted. Figure 9(a) shows a photograph of a measured skin region including veins and Fig. 9(b) a classical ultrasound image (B-mode) along with the dashed line in Fig. 9(a). We can confirm the positions of veins as two dark elliptical spots in Fig. 9(b). The distance between the center of the two spots or veins is about 12 mm. The depth from the skin surface to the top of the left vein is 1.3 mm, whereas that for the right vein is 1.5 mm. We evaluated the thickness (diameter) around the center of each vein as $t=0.54$ to 1.2 mm for the left one and $t=0.51$ to 0.85 mm for the right one.

Figure 10 demonstrates images obtained by the proposed method for volume concentration of melanosomes C_m in epidermis [Fig. 10(a)] and that of blood C_b in dermis [Fig. 10(b)]. In Figs. 10(a) and 10(b), we used the rectangular area enclosed by a dashed line as site A to estimate the averaged concentrations C_m and C_b. The estimated values of C_m and C_b were 0.71 and 0.90%, respectively, which are close to values reported in the literature.[19,33] Figure 10 also shows 2-D distributions for depth [Fig. 10(c)] and thickness of veins obtained by the proposed method [Fig. 10(d)]. However, the border of veins is blurred as we supposed from the phantom experiment. Figure 11 shows profiles of depth [Fig. 11(a)] and thickness [Fig. 11(b)] along with the dashed lines in Figs. 10(c) and 10(d), respectively. In both of Figs. 11(a) and 11(b), the distance between two peaks is about 12 mm, which corresponds to the result from the conventional ultrasound shown in Fig. 9(b). Discrepancy between the estimated values from the proposed method and the ultrasound technique are 0.25 to 0.6 mm for depth and 0.1 to 0.2 mm for thickness. Therefore, the current measurement has the average errors of 30% for depth and 19% for thickness. These errors are probably due to discrepancy in optical properties between the actual human skin and the skin tissue model assumed in the Monte Carlo simulations. This issue is discussed in Sec. 4.3.

Figure 11(c) shows an outline profile that combines the profiles of d and t. Plots of squares and circles denote the

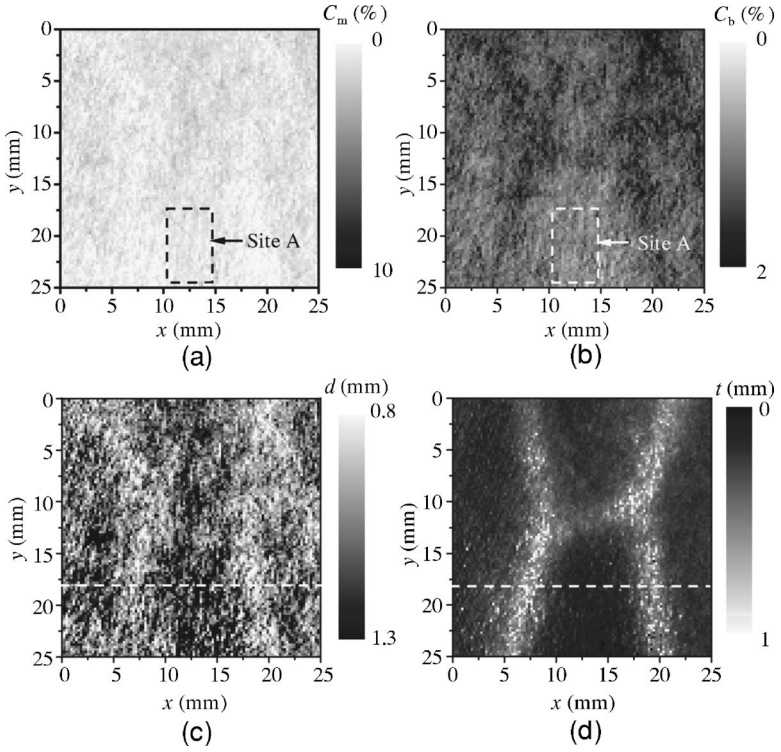

Fig. 10 Concentration images of (a) melanosomes in epidermis and (b) blood in dermis, obtained from human skin tissue. Rectangular areas enclosed by the dashed line were used as site A to estimate the averaged values of C_m and C_b. Images of (c) depth and (d) thickness of human veins.

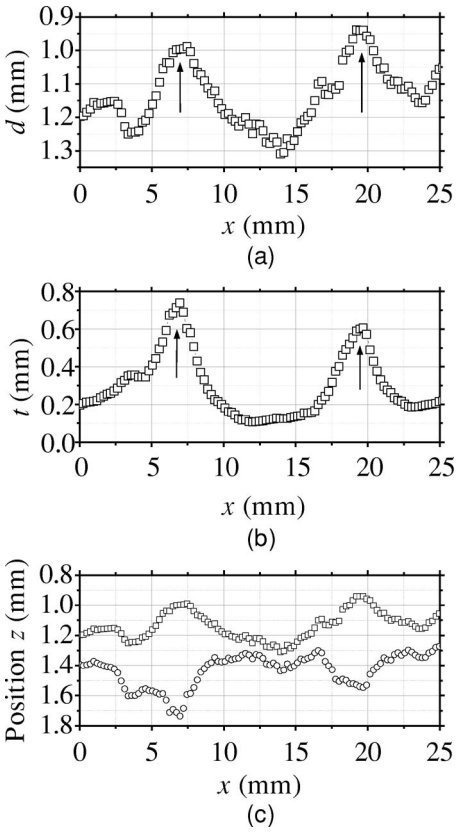

Fig. 11 Profiles of (a) depth and (b) thickness corresponding to the dashed line in Figs. 10(c) and 10(d), respectively. Arrows indicate the actual positions of veins. (c) Outline profile of the veins reconstructed from (a) and (b).

estimated upper and lower borders of veins, obtained from Figs. 11(a) and 11(b), respectively. There are two possible regions that are supposed to be veins. Separation of veins and surrounding tissue is not clear, as shown in Fig. 11(c). This may be due to the diffusion effect of light in addition to the discrepancy between the actual human skin and the skin tissue model in the Monte Carlo simulation. These problems could prevent the method from reconstructing the outline of veins having complex shape and distribution. Assuming a cylindrical blood region model, incident light may diffuse around the blood region and give lower *OD* value than that for the simple solid layer model. This diffusion effect could be strong at the longer wavelengths (585 or 800 nm) where a tissue scattering coefficient is low compared to that at the shorter wavelength (420 nm). As a consequence, both $r_1(=OD_{420}/OD_{585})$ and $r_2(=OD_{420}/OD_{800})$ decrease, and thus the depth and thickness may be over- and underestimated, respectively. Moreover, as supposed from the results of phantom experiments, these errors could be more remarkable near the lateral borders of the local blood region. The blurring effect may possibly be corrected by a phantom including a vein-like cylindrical blood region with known depth and diameter, as developed by Kienle et al.[34] Practically, it may also be improved by image processing based on 2-D deconvolution using the point-spread function. It should be noted that the resultant images from the human skin suffered from some fine glares due to the surface roughness of tissue. Those glares could not be seen in the results of the phantom, which was naturally coupled to and covered with the slide glass by water. Use of polarizers may be effective to reduce deterioration of image quality due to the glare.[35] Details of these issues will be studied in our future work.

Table 3 Results of C_m and C_b for different variations in $\mu_s(\lambda)$ of skin tissue.

	Variation [%] in $\mu_s(\lambda)$	C_m [%]	C_b [%]
Given	–	4.0	0.2
Estimated	−20	4.34	0.21
	−10	4.11	0.21
	10	3.90	0.19
	20	3.68	0.2

4.3 *Numerical Investigation*

Table 3 demonstrates results of C_m and C_b obtained for four different variations in $\mu_s(\lambda)$ mm^{-1} of skin tissue. The estimated value of C_m decreases as the variation in $\mu_s(\lambda)$ changes from negative to positive, while that of C_b has no significant change. A large variation in $\mu_s(\lambda)$ is found to cause deviation of C_m. This result is originated from changes of *OD* or *R* due to variations of μ_s at 420 and 585 nm. Figure 12(a) shows

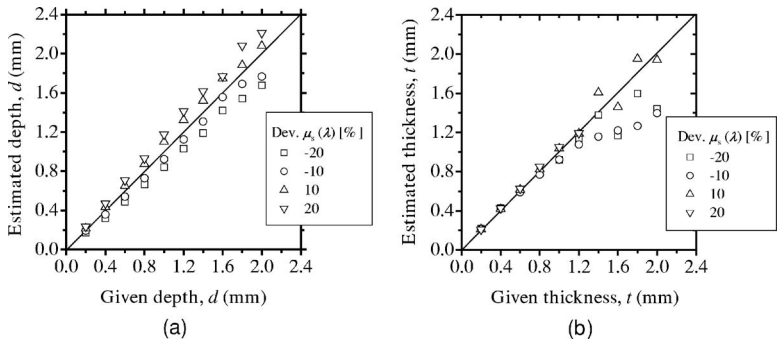

Fig. 12 Comparison of estimated and given values of (a) depth and (b) thickness of a local blood region for different variations in $\mu_s(\lambda)$ of skin tissue, obtained from numerical investigations.

Table 4 Results of C_m and C_b for different variations in Hct of blood.

	Variation [%] in Hct	C_m [%]	C_b [%]
Given	–	4.0	0.2
Estimated	−20	3.99	0.16
	−10	4.11	0.17
	14	3.96	0.23
	25	3.98	0.26

numerical comparison of depth d and Fig. 12(b) shows the thickness t of the blood region. In Fig. 12(a), the depth d is over- or underestimated as $\mu_s(\lambda)$ decreases or increases from the typical value. This result may be attributed by two factors. One is fluctuation of the function $r_1(d)$ due to the error of C_m, which can be interpreted by Eqs. (11) through (14). Another is the error in the OD ratio r_1 at site B, which is caused by the variation of $\mu_s(\lambda)$ from the typical value. Since the scattering coefficient of human skin tissue at the shorter wavelength is larger than that at the longer, the value of OD_{420} is more sensitive than that of OD_{585} to the deviation of $\mu_s(\lambda)$. If $\mu_s(\lambda)$ becomes small or large compared to the typical one, the value of r_1 at site B increases or decreases. Such fluctuations of r_1 were considered to yield errors of d in Fig. 12(a). On the other hand, in Fig. 12(b), the estimated values of t below 1.2 mm agree well with the given values. This result is because errors of C_m, C_b, and d are cancelled out in derivation of the function $r_2(t)$.

Table 4 shows results of C_m and C_b obtained for four different variations in Hct value of blood. The estimated value of C_b increases significantly as the variation in Hct changes from negative to positive, while that of C_m shows no systematic change. This is due to the following consideration. Most 420-nm light may be absorbed by melanosomes in epidermis, whereas the light at 585-nm wavelength easily penetrates the deeper region of dermis and is sufficiently absorbed by the blood in dermis. Although the hemoglobin absorbs the light at 420 nm strongly, the probability that light is absorbed in dermis is weaker at 420 nm than at 585 nm. Thus, OD_{420} at site A reflects less of the variation in hematocrit of blood distributed in the dermis, but OD_{585} does significantly. As a consequence, the estimated value of C_b depends on the Hct value. Figure 13(a) shows results of depth d and Fig. 13(b) shows the thickness t of the blood region. The estimated thickness t has relatively large deviation from the given value, whereas the variation in Hct value has almost no influence on the estimated depth d. In Fig. 13(b), the thickness t is over- or underestimated when the Hct value decreases or increases from the typical value. The contribution of absorption in the local blood region to the reflectance is higher at 800 nm than that at 585 nm. Therefore, the deviation of OD_{800} becomes large in comparison with that of OD_{585}. This means that $r_2(t)$ is more sensitive than $r_1(d)$ to absorbing conditions in the local blood region, and thus, the errors in thickness t are more remarkable than that in depth d. It should be mentioned that a combined uncertainty of Hct and $\mu_s(\lambda)$ may add up to a larger relative error in depth d and thickness t. As seen in Fig. 12(b), for instance, a variation in $\mu_s(\lambda)$ of 20% at $t=1.6$ mm can be estimated as a relative error of roughly 30%. Similarly, a variation in Hct of 20% also gives a relative error of roughly 30%. A combination of the two uncertainties may give a considerably larger relative error in the thickness t. Errors in thickness t above 1.2 mm shown in Figs. 12(b) and 13(b) may be because it is out of the measurable range in the function $r_2(t)$, as shown in Fig. 2(b).

The proposed method depends on many assumptions and simplifications. Therefore, the expected effects of the assumptions and simplifications on the results should be taken into consideration for *in-vivo* skin measurements in the future. In this study, we assumed that a local blood region is filled with whole blood with 44% hematocrit. This assumption is suitable for experiments with *in-vivo* skin tissue. However, the port wine stains and tumors may have lower volume concentration of blood than usual veins. Such a difference in the blood concentration, i.e., absorption of a local blood region, can cause misestimation, especially in thickness, as shown in the numerical results. Absorption of melaninless epidermis and bloodless dermis were not taken into consideration in absorption coefficients of epidermis and dermis, respectively, in this study. Therefore, the volume concentrations of melanin in epidermis C_m and blood in dermis C_b may be overestimated in Figs. 10(a) and 10(b).

In the previous work by Verkruysse et al.,[36] it has been shown that when blood is modeled to be homogeneously distributed over the dermis, fewer red blood cells would produce

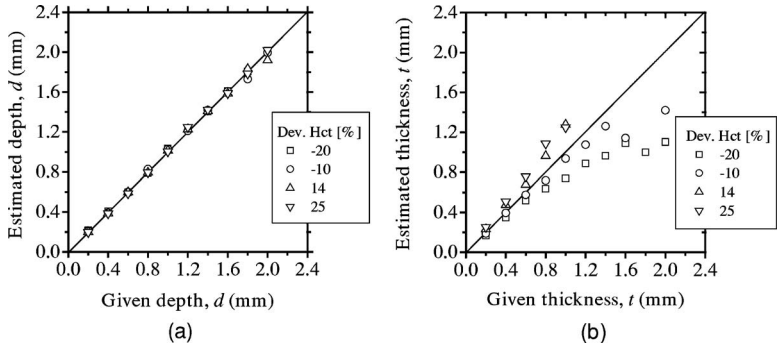

Fig. 13 Comparison of estimated and given values of (a) depth and (b) thickness of a local blood region for different variations in Hct of blood, obtained from numerical investigations.

the same absorption as the actual number of red blood cells distributed in the discrete vessels. Their results indicate that the optical density (OD) of the homogeneously distributed model could be higher than that of the discrete vessel model for the same concentration of blood. This effect may be strong where the optical absorption of blood is high at 420 nm and weak at 585 nm, and negligible at 800 nm. Therefore, the function $r_1(d)$ and $r_2(t)$ for the discrete vessel model will be shifted downward, compared to those for the homogeneously distributed model shown in Figs. 2(a) and 2(b). As a consequence, the estimated values of depth or thickness in the discrete vessel model may be under- or overestimated, respectively. The presence of capillaries localized in epidermal ridges in the papillary dermis would also affect the absorption of blood at 420 nm, and may give a similar situation to the discrete vessel model. This would cause the overestimation of C_b, and thus give the under- or overestimation of depth d or thickness t in the homogeneously distributed blood model.

The epidermal ridges lie between the epidermis and dermis, and thus, the epidermis and dermis are not flat actually. Also, since the cell structures and their sizes for epidermis and dermis are different, the contributions of Rayleigh scattering and Mie scattering to these layers are not the same. Therefore, there should strictly be some differences between the epidermis and dermis both in $\mu_s(\lambda)$ and $g(\lambda)$. Nevertheless, we assumed that the scattering properties of epidermis and dermis are the same and calculated them by Eqs. (4) and (5) for convenience. The shape of epidermal ridges and the differences between the epidermis and dermis in $\mu_s(\lambda)$ and $g(\lambda)$ are of great importance for methods and techniques that mainly depend on single backscattering, coherent backscattering, or polarized backscattering. On the other hand, details of the ridge and differences of the scattering properties between the epidermis and dermis may be of minor importance for visible and near-infrared applications with diffusive light distribution, such as the proposed method. In fact, there are some approaches based on flat layered skin models[6,7,13,14,16,17,30] and a model[30] that treats the epidermis and dermis identically in terms of $\mu_s(\lambda)$ and $g(\lambda)$. Modeling of skin tissue using more reliable structural and optical parameters is necessary for deducing the depth and thickness accurately. More strict validation of the results such as a histology comparison should be made to establish the proposed method with reliable accuracy.

5 Conclusion

In summary, we demonstrate a new visualizing method for both depth and thickness of a local blood region based on reflectance images at three isosbestic wavelengths of 420, 585, and 800 nm. The empirical formulas for the depth and thickness are established by diffuse reflectance samples generated by the Monte Carlo simulation of light transport for layered skin tissue structure. The feasibility of the method is shown by experiments with tissue-like agar gel phantoms and human skin veins. Expected errors due to the variations in the scattering coefficient of skin tissue and the hematocrit of blood are investigated by Monte Carlo simulation. This method probes the depth and thickness, that is, structural outline of the local blood region in which the absorption coefficient is assumed to be uniform. In this point, the technique differs from other techniques such as diffuse optical tomography or optoacoustic imaging that visualize inhomogeneity of the absorption coefficient within the tissue. For practical uses, it is desirable to estimate also the scattering coefficient of skin tissue and hematocrit of the blood in a framework of this method. This subject should be studied in a future work by performing further experiments on animals and tissue models with various optical and structural properties.

Acknowledgment

Part of this work was supported by Grant-in-Aid for Scientific Research from the Japan Society for the Promotion of Science.

References

1. M. Poetke, "Laser treatment in haemangiomas and vascular malformations," in *Applied Laser Medicine*, H. P. Berlien and G. J. Müller, Eds., pp. 443–482, Springer-Verlag, Berlin (2003).
2. C. T. W. Lahaye and M. J. C. van Gemert, "Optimal laser parameters for port wine stain therapy: a theoretical approach," *Phys. Med. Biol.* **30**, 573–587 (1985).
3. M. J. C. van Gemert, A. J. Welch, and A. P. Amin, "Is there an optimal laser treatment for port wine stains?," *Lasers Surg. Med.* **6**, 76–83 (1986).
4. J. W. Pickering, P. H. Butler, B. J. Ring, and E. P. Walker, "Thermal profiles of blood vessels heated by a laser," *Australas. Phys. Eng. Sci. Med.* **12**, 11–15 (1989).
5. J. W. Pickering, P. H. Butler, B. J. Ring, and E. P. Walker, "Computed temperature distributions around ectatic capillaries exposed to yellow (578 nm) laser light," *Phys. Med. Biol.* **34**, 1247–1258 (1989).
6. W. Verkruysse, J. W. Pickering, J. F. Beek, M. Keijzer, and M. J. C. van Gemert, "Modeling the effect of wavelength on the pulsed dye laser treatment of port wine stains," *Appl. Opt.* **32**, 393–398 (1993).
7. J. W. Tunnell, L. V. Wang, and B. Anvari, "Optimum pulse duration and radiant exposure for vascular laser therapy of dark port-wine skin: a theoretical study," *Appl. Opt.* **42**, 1367– 1378 (2003).
8. J. S. Nelson, T. E. Milner, B. S. Tanenbaum, D. M. Goodman, and M. J. C. van Gemert, "Infra-red tomography of port-wine-stain blood vessel in human skin," *Lasers Med. Sci.* **11**, 199–204 (1996).
9. B. P. Payne, V. Venugopalan, B. B. Mikić, and N. S. Nishioka, "Optoacoustic tomography using time-resolved interferometric detection of surface displacement," *J. Biomed. Opt.* **8**, 273–280 (2003).
10. R. O. Esenaliev, A. A. Karabutov, and A. A. Oraevsky, "Sensitivity of laser opto-acoustic imaging in detection of small deeply embedded tumors," *IEEE J. Sel. Top. Quantum Electron.* **5**, 981–987 (1999).
11. X. Wang, Y. Pang, G. Ku, G. Stoica, and L. V. Wang, "Three-dimensional laser-induced photoacoustic tomography of mouse brain with the skin and skull intact," *Opt. Lett.* **28**, 1739–1741 (2003).
12. M. G. Sowa, J. R. Payette, M. D. Hewko, and H. H. Mantsch, "Visible-near infrared multispectral imaging of the rat dorsal skin flap," *J. Biomed. Opt.* **4**, 474–481 (1999).
13. N. Tsumura, H. Haneishi, and Y. Miyake, "Independent-component analysis of skin color image," *J. Opt. Soc. Am. A* **16**, 2169–2176 (1999).
14. M. Shimada, Y. Masuda, Y. Yamada, M. Itoh, M. Takahashi, and T. Yatagai, "Explanation of human skin color by multiple linear regression analysis based on the modified Lambert-Beer law," *Opt. Rev.* **7**, 348–352 (2000).
15. A. A. Stratonnikov and V. B. Loschenov, "Evaluation of blood oxygen saturation *in vivo* from diffuse reflectance spectra," *J. Biomed. Opt.* **6**, 457–467 (2001).
16. M. Shimada, Y. Yamada, M. Itoh, and T. Yatagai, "Melanin and blood concentration in human skin studied by multiple regression analysis: experiments," *Phys. Med. Biol.* **46**, 2385–2395 (2001).
17. M. Shimada, Y. Yamada, M. Itoh, and T. Yatagai, "Melanin and blood concentration in human skin studied by multiple regression analysis: assessment by Monte Carlo simulation," *Phys. Med. Biol.* **46**, 2397–2406 (2001).
18. I. Nishidate, Y. Aizu, and H. Mishina, "Estimation of absorbing components in a local blood layer embedded in the turbid media on the basis of visible to near-infrared (VIS-NIR) reflectance spectra," *Opt. Rev.* **10**, 427–435 (2003).

19. I. Nishidate, Y. Aizu, and H. Mishina, "Estimation of melanin and hemoglobin in skin tissue using multiple regression analysis aided by Monte Carlo simulation," *J. Biomed. Opt.* **9**, 700–710 (2004).
20. P. B. Bargo, S. A. Prahl, T. T. Goodell, R. A. Sleven, G. Koval, G. Blair, and S. L. Jacques, "In vivo determination of optical properties of normal and tumor tissue with white light reflectance and an empirical light transport model during endoscopy," *J. Biomed. Opt.* **10**, 034018 (2005).
21. T. Iwai and G. Kimura, "Imaging of an absorbing object embedded in a dense scattering medium by diffusing light topography," *Opt. Rev.* **7**, 436–441 (2000).
22. S. L. Jacques, I. S. Saidi, and F. K. Tittel, "Average depth of blood vessels in skin and lesions deduced by optical fiber spectroscopy," *Proc. SPIE* **2128**, 231–237 (1994).
23. I. Nishidate, Y. Aizu, and H. Mishina, "Depth visualization of a local blood region in skin tissue by use of diffuse reflectance images," *Opt. Lett.* **30**, 2128–2130 (2005).
24. L. H. Wang, S. L. Jacques, and L. Q. Zheng, "MCML-Monte Carlo modeling of photon transport in multi-layered tissues," *Comput. Methods Programs Biomed.* **47**, 131–146 (1995).
25. S. L. Jacques and D. J. McAuliffe, "The melanosome: threshold temperature for explosive vaporization and internal absorption coefficient during pulsed laser irradiation," *Photochem. Photobiol.* **53**, 769–775 (1991).
26. S. A. Prahl, *Tabulated Molar Extinction Coefficient for Hemoglobin in Water*, see http://omlc.ogi.edu/spectra/hemoglobin/summary.html(1999).
27. A. Roggan, M. Friebel, K. Dörschel, A. Hahn, and G. Muller, "Optical properties of circulating human blood in the wavelength range 400-2500 nm," *J. Biomed. Opt.* **4**, 36–46 (1999).
28. S. L. Jacques, *Skin Optics*, see http://omlc.ogi.edu/news/jan98/skinoptics.html(1998).
29. M. J. C. van Gemert, S. L. Jacques, H. J. C. M. Sterenborg, and W. M. Star, "Skin optics," *IEEE Trans. Biomed. Eng.* **36**, 1146–1154 (1989).
30. T. Dai, B. M. Pikkula, L. V. Wang, and B. Anvari, "Comparison of human skin opto-thermal response to near-infrared and visible laser irradiations: a theoretical investigation," *Phys. Med. Biol.* **49**, 4861–4877 (2004).
31. I. Nishidate, T. Maeda, Y. Aizu, K. Niizeki, and H. Mishina, "Visualization of depth and thickness of a local blood region in skin tissue using diffuse reflectance images," *Proc. 6th Japan-Finland Joint Symposium on Optics in Engineering*, Sapporo, Japan, 2004, pp. 59-60.
32. H. J. van Staveren, C. J. M. Moes, J. Marle, S. A. Prahl, and M. J. C. Gamert, "Light scattering in Intralipid-10% in the wavelength range of 400-1100 nm," *Appl. Opt.* **30**, 4507–4514 (1991).
33. S. L. Jacques, R. D. Glickman, and J. A. Schwartz, "Internal absorption coefficient and threshold for pulsed laser disruption of melanosomes isolated from retinal pigment epithelium," *Proc. SPIE* **2681**, 468–477 (1996).
34. A. Kienle, L. Lilge, I. A. Vitkin, M. S. Patterson, B. C. Wilson, R. Hibst, and R. Steinner, "Why do veins appear blue? A new look at an old question," *Appl. Opt.* **35**, 1151–1160 (1996).
35. S. L. Jacques, J. C. Ramella-Roman, and K. Lee, "Imaging skin pathology with polarized light," *J. Biomed. Opt.* **7**, 329–340 (2002).
36. W. Verkruysse, G. W. Lucassen, J. F. de Boer, D. J. Smithies, J. S. Nelson, and M. J. C. van Gemert, "Modeling light distributions of homogeneous versus discrete absorbers in light irradiated turbid media," *Phys. Med. Biol.* **42**, 51–65 (1997).